iScience

Article

# Global potential of continuous sorption-based atmospheric water harvesting

## Graphical abstract

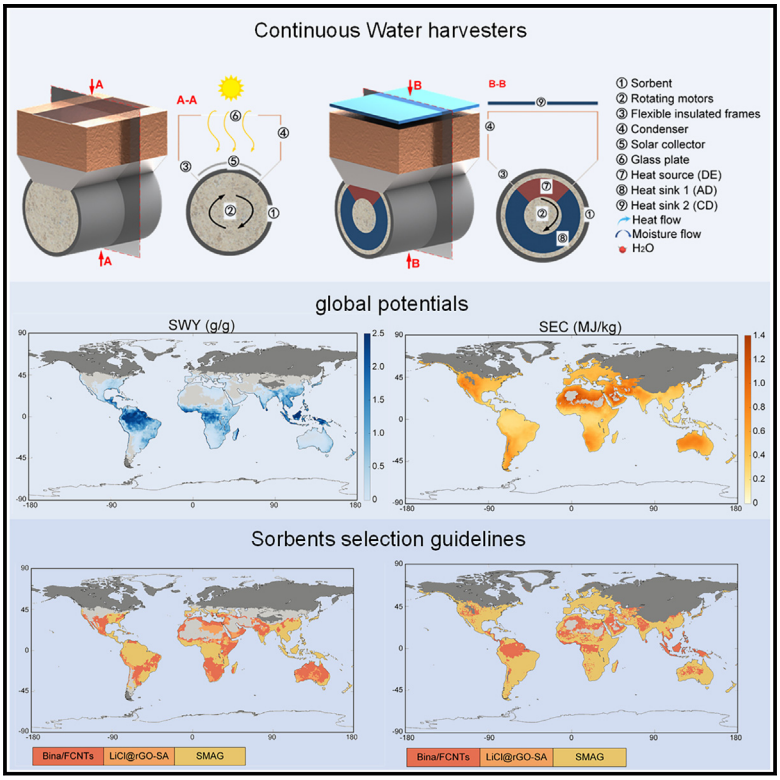


## Highlights

- Establishment of thermodynamic model of active/passive SAWH system
- Assessment of global water potential through high-resolution meteorological data
- Proposal of adsorbent deployment strategy and development pathway

## Authors

Wenjun Ying, Chunfeng Li, Liang Yang, Lingji Hua, Hua Zhang, Ruzhu Wang, Jiayun Wang

## Correspondence

jywang@usst.edu.cn

## In brief

Environmental science; Energy Modeling; Water resources engineering

Ying et al., 2025, iScience *28*, 112160
April 18, 2025 
https://doi.org/10.1016/j.isci.2025.112160

CellPress

iScience

CellPress
OPEN ACCESS

Article

# Global potential of continuous sorption-based atmospheric water harvesting

Wenjun Ying,[1] Chunfeng Li,[1] Liang Yang,[2] Lingji Hua,[3] Hua Zhang,[1] Ruzhu Wang,[3] and Jiayun Wang[1,4,*]
[1]Institute of Refrigeration and Cryogenics, University of Shanghai for Science and Technology, Shanghai 200093, China
[2]Shanghai Key Laboratory of Multiphase Flow and Heat Transfer in Power Engineering, University of Shanghai for Science and Technology, Shanghai 200093, China
[3]Institute of Refrigeration and Cryogenics, Shanghai Jiao Tong University, 800 Dongchuan Road, Shanghai 200240, China
[4]Lead contact
*Correspondence: jywang@usst.edu.cn
https://doi.org/10.1016/j.isci.2025.112160

## SUMMARY

Sorption-based atmospheric water harvesting (SAWH) offers a decentralized solution for freshwater generation in remote and arid regions. Continuous SAWH systems, with their compact design and energy efficiency, present advantages over discontinuous systems for kilogram-scale water supply. Using global meteorological data and advanced modeling, we evaluated the performance of passive and active continuous systems, incorporating the isothermal and dynamic properties of twelve advanced sorbents, such as hydrogels, metal-organic frameworks, and composites. Results show that solar-powered continuous SAWH systems can operate effectively year-round in 39.53% of global districts, while active systems enable low-energy harvesting in 55.27% of districts. Temperature and humidity significantly influence performance, with correlations of 47.41% and 86.41%, respectively, surpassing the impact of atmospheric pressure and solar radiation. This study provides a predictive framework for global SAWH performance, offering design insights to optimize system efficiency and guide sorbent development for broader applications.

## INTRODUCTION

Freshwater scarcity is a critical global issue that poses a significant threat to social and economic development.[1] With industrial development, human activities, such as agricultural irrigation, industrial production, and daily life, have become increasingly dependent on freshwater resources, leading to their pollution and exacerbating water scarcity.[2,3] To address this problem, research on innovative technologies such as desalination and atmospheric water harvesting (AWH) must be promoted. Unlike seawater desalination,[4] which is primarily applicable in coastal areas, AWH technologies[5] represent a decentralized approach to freshwater production. AWH technologies extract water from the air through methods such as fog harvesting,[6] dew collection,[7] membrane systems,[8] and sorbent-based processes.[9] Although the operational efficiency of AWH technologies is inherently constrained by environmental factors, sorbent-assisted AWH (SAWH) exhibits distinct advantages over alternative methods, particularly in low-humidity environments. Other methods, such as fog harvesting (limited to supersaturated conditions) or dew harvesting (ineffective below freezing), face greater limitations.[10]

The performance of SAWH systems is considerably influenced by the characteristics of the adsorbent. Various adsorbents such as hygroscopic salts,[11] zeolites with large pore sizes,[12] covalent organic frameworks (COFs),[13] and metal-organic frameworks (MOFs)[14–18] have been developed and investigated. However, many of these absorbents suffer from limitations such as low water adsorption capacity, low adsorption rates, and high desorption energy requirements. In comparison, hygroscopic hydrogels[19,20] are a promising option for SAWH due to their unique polymer network. They can realize chemisorption and capture moisture through hydrogen bond formation, electronic interactions, or covalent interactions.[21] The porous substrate of hydrogels facilitates water storage and encapsulation, resulting in fast kinetics, high water uptake capacity, and low desorption enthalpy, thereby effectively addressing the limitations of other adsorbents. Furthermore, the polymer networks can exhibit distinctive hydrogel properties, including temperature-sensitive switching between hydrophilicity and hydrophobicity.[22] Additionally, polymer networks enable the incorporation of materials such as hygroscopic salts and photo-thermal factors to achieve more specific properties.[23,24] The versatile nature of these properties means that hydrogels have a wide range of applications in the energy and water-related industries.

To ensure efficiency, it is important to design continuous water harvesting systems appropriately.[25] Unlike earlier systems[26,27] that relied on adsorption at night and desorption during the day, the operation of continuous systems does not depend on diurnal cycle variations, which promotes continuous water production. For example, Li et al.[28] proposed a partially closed condensing system with the adsorbent mounted in a rotating cylinder in the middle to ensure continuous water production via solar energy. Xiang et al.[23] achieved continuous water extraction

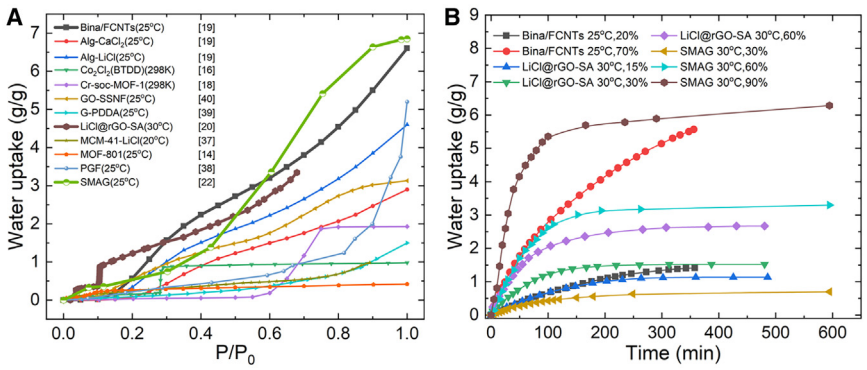


**Figure 1. Water adsorption properties of selected adsorbents**

(A) Isotherms of twelve adsorbents; the three bold lines represent the sorbents used in this study.

(B) Dynamic adsorption characteristics in different operating conditions.

by cyclic desorption of two pieces of adsorbent alternately. However, continuous systems place higher demands on adsorbent kinetics. To maximize the potential of the adsorbent, it is important to match the adsorption and desorption kinetics to the operating mode of the continuous system.

Another bottleneck to the widespread use of AWH systems is that their design must be optimized according to environmental conditions.[29] Previous studies have developed various thermodynamic frameworks for AWH and have shown that adjusting the heat source can improve the system's efficiency.[30–32] There is still a lot of doubt surrounding the efficiency of water extraction at low relative humidity (RH) for SAWH. Furthermore, due to the fluctuating climate of a region, it can be challenging to determine the performance of adsorbents in a given situation through performance testing alone. Lord et al.[33] first demonstrated the global potential of SAWH by analyzing the performance of solar-driven water harvesting systems. Kocher et al.[34] performed an economic comparison between desalination and AWH, showing that the economic pressure on AWH comes primarily from energy consumption. Rao et al.[35] conducted an energy analysis that suggests the superiority of adsorptive airborne water harvesting in low humidity. However, it should be noted that these studies usually focus on MOFs materials, while the impact of gel materials has not been widely studied. Furthermore, it is crucial to distinguish between the evaluation criteria for passive and active systems, as they differ. Subsequently, the adsorbent's performance is proven and benchmarks for its applicability are established by calculating the standard values for the different materials.

To address these problems, we used meteorological data to develop reliable quantitative analysis models to evaluate the potential of different advanced sorbents in continuous SAWH systems. The proposed models comprehensively consider the isothermal and dynamic properties of twelve types of state-of-the-art sorbents and the operating characteristics of a continuous system. Based on the properties of adsorbents, an algorithm is proposed to optimize the operation mode of the continuous systems using different adsorbents to improve performance. We proposed two indices to evaluate the performance of continuous SAWH systems: specific water yield (SWY) for passive systems and specific energy consumption (SEC) for active systems. Using high-precision weather data from 2022, we assessed the potential of the different sorbents at the system level with these two indicators and mapped the results of average performance. We considered three typical arid regions and examined the possibility of adapting the sorbents to the seasonal variations. The findings demonstrate that the continuous SAWH system can effectively perform solar-powered water harvesting year-round in 39.53% of districts while enabling low-energy harvesting through active components in 55.27% of districts. Furthermore, the effects of temperature and humidity on the performance were more notable than those of atmospheric pressure and solar radiation intensity, with a correlation of 47.41% and 86.41%, respectively. These outcomes provide critical insights for the deployment of hygroscopic hydrogels across various regions and offer directions for their future development. Additionally, our findings can inform optimization strategies to harness the full potential of SAWH technologies, presenting a practical solution to address drought-related challenges in water-scarce areas.

## RESULTS

### Sorbent selection

The static adsorption characteristics refer to the amount of adsorption when an adsorbent reaches a steady state at a specific temperature and RH. The adsorption isotherm serves as a metric to assess the static performance of the adsorbent material and can indicate the potential applications of the adsorbent in various operating conditions. According to the classification system established by the International Union of Pure and Applied Chemistry, the isotherms of all adsorbents can be divided into six types (Figure S1A).[36]

For the analysis, we selected twelve state-of-the-art sorbent materials, including MOFs (MOF-801,[14] $Co_2Cl_2$(BTDD),[16] and Cr-soc-MOF-1[18]), a salt-based composite (MCM-41-LiCl[37]), two aerogels (PGF,[38] G-PDDA[39]), a nanomembrane (GO-SSNF[40]), and hydrogel sorbents. These materials have undergone stability testing over multiple cycles and have proven stable for freshwater production applications. Table S1 displays the specific test conditions and stability. The isotherms shown in Figure 1A illustrate that hydrogel sorbents have higher water uptake than the other adsorbents. Thus, we selected the three hydrogel sorbents with the highest water uptake in hygroscopic gels as the research objects: Bina/FCNTs[19] (1.57–3.2–5.5 g/g at RH 30%–60%–90%), LiCl@rGO-SA[20] (1.5–3.3 g/g at RH 30%–60%), and Super Moisture-Absorbents Gels[22] (SMAG, 0.7–3.4–6.0 g/g at RH 30%–60%–90%).

Another factor that affects the performance of continuous water harvesting systems is the adsorption kinetics, which determines, to a certain extent, the number of cycles per day and

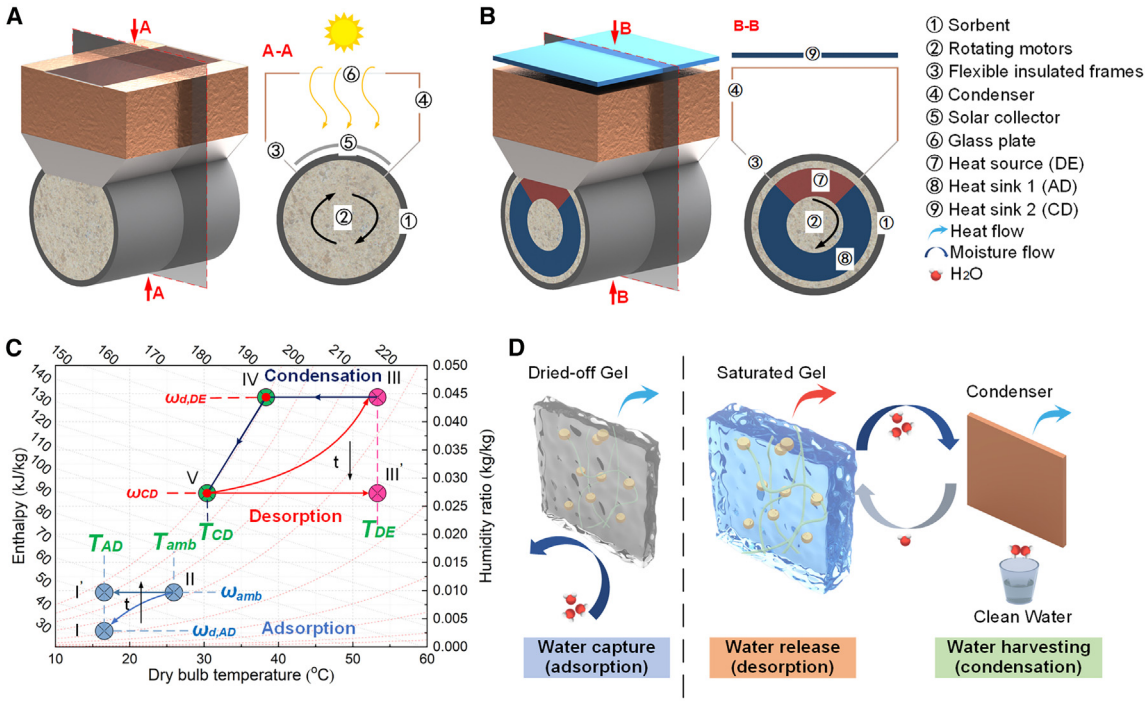


**Figure 2. Operating principle of the continuous SAWH systems and basis for the thermodynamic framework**

(A) Conceptual design of a passive continuous water harvesting system, based on existing devices.

(B) Active device with the condensing wall surface fully closed. Electric heating supplies the energy for the three heat sources/sinks provided by electric heating.

(C) Air treatment process of sorption-based AWHs.

(D) Heat and moisture transfer processes in hygroscopic hydrogels.

the actual amount of water adsorbed at a given time. As shown in Figure 1B, the adsorption kinetics determines the rate at which adsorbents reach saturation. The macroscopic dynamics are affected by the ambient temperature, RH, adsorption bed filling density, and material porosity.[41,42] In practice, it is difficult to determine the adsorption rate in the given operating conditions directly. Therefore, it is necessary to define an average adsorption/desorption rate for different conditions. To this end, we used the linear driving force (LDF) equation (detailed in STAR Methods). To determine the accuracy of this equation, we calculated the adsorption and desorption rates in different working conditions, as shown in Figures S1B and S1C. The error of the dynamic constant in different working conditions was within 5%. Notably, because the desorption rates are typically higher than adsorption rates, they must be calculated separately.

## Model framework

Figures 2A and 2B show two conceptual designs of continuous SAWH systems. The main structure of the ideal physical model consists of a cylinder, a desorption-condensing chamber, and a flexible sealing plate that connects these two parts. The cylinder is coated with the sorbent and rotated by a rotating motor at a constant rate. The sealing plate is designed to be both adiabatic and hermetic, preventing the exchange of heat and moisture between the adsorption and desorption zones. Additionally, it is flexible enough to allow the adsorbent to rotate without interruption. The condenser is designed to condense hot moist air and collect liquid droplets. Based on the model, Figures S2–S4 illustrate the small validation device we constructed to verify the feasibility of the drum design for heat and mass transfer, as well as the top condensation design.

The two systems are powered by different sources. The system shown in Figure 2A is a solar-powered passive system and cross-section A–A shows its internal components. At the top, a transparent glass panel acts as a seal, allowing sunlight to penetrate. Above the sorbent, a solar collector converts solar irradiation to heat, facilitating the overall process. In contrast, the system depicted in Figure 2B is powered by three active energy sources. In cross-section B–B, the cylinder has a central annular zone that is divided according to the prescribed configuration, corresponding to the proportions of the adsorption and desorption zones. The red and blue regions of the ring represent a stationary heat source for assisted desorption and a stationary cooler for assisted adsorption, respectively. Both regions remain stationary. In addition, a heat sink is placed above the condenser to dissipate the condensation heat. Owing to these design variations, the mathematical models for the two devices are different: the input and output of passive devices are solar irradiation intensity and maximum water extraction, respectively. In contrast, active devices adjust the temperature of the three heat/cold sources to achieve a fixed amount of water harvesting and minimize the energy requirements.

The workflows of both active and passive SAWH systems are shown in Figure 2C. In the initial stage of adsorption, the

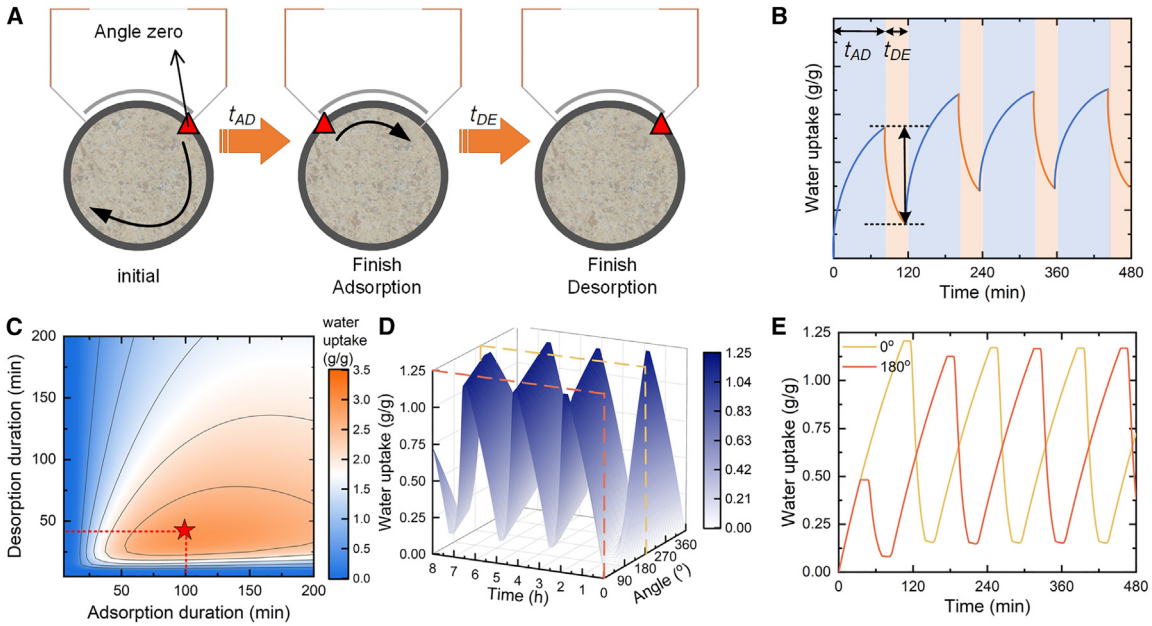


**Figure 3. Single-day water extraction strategy for a passive system**

(A) Schematic diagram of cylinder rotation. The red triangle is defined as angle zero.

(B) Schematic diagram of water uptake of angle zeros within 8 h.

(C) The optimization program plots contours of daily water release from Bina/FCNTs under 30°C, 60% RH based on adsorption and desorption time. The red pentagram is the optimal point, corresponding to adsorption and desorption times of 65 and 20 min, respectively.

(D) Change in the water uptake for the entire Bina/FCNTs at optimal operating mode.

(E) Change in the water uptake of the Bina/FCNTs at 0° and 180°.

adsorbent is at the adsorption temperature $T_{AD}$. Then, as air flows through the adsorbent, moisture is transferred due to the difference between the moisture contents of the air and the adsorbent. Once the humidity ratio of the air and adsorbent are equal ($\omega_{d,AD} = \omega_{amb}$), the adsorbent can no longer continue to absorb moisture from the air. It is important to note that for continuous systems, this condition does not necessarily need to be met before desorption takes place, and the optimal mode of operation needs to be selected based on the properties of the material under consideration. During adsorption, the air exit state gradually moves upwards along the $T_{AD}$, and the moisture content of the adsorbent increases (Figures 2D and S5). Subsequently, the adsorbent still contains the same amount of water as adsorbed in the adsorption stage but warms up to the desorption temperature $T_{DE}$. During desorption, the air temperature and humidity increase due to the differences in the temperature and moisture contents of the adsorbent and air. As the air flows through the condenser, it cools to the saturation RH line and then follows it to attain the condensation temperature $T_{CD}$ (blue-green line with arrow in Figure 2C). At this point, the difference in the humidity ($\omega_{d,DE}$ and $\omega_{CD}$) is the amount of water obtained in this condensation cycle. This air then flows back to the high-temperature adsorbent beds and is desorbed again (red line with arrow), thereby completing one desorption-condensation cycle. The final amount of water obtained, $\Delta W$ (also known as *SWY*), is the difference in the moisture content of the adsorbent at the end of adsorption and that at the end of desorption. This amount can also be expressed as the sum of the water obtained in multiple desorption-condensation cycles. Details of this process can be found in STAR Methods.

## Operating mode

The operating mode of the system is significantly related to the dynamic performance of the adsorbent. In a mathematical model of a passive system, the operation mode serves as a potential input. The water yields are enhanced when the adsorbent is compatible with the environment and the system operation mode is aligned with its properties. However, in an active system, the input is defined as the amount of water that yields, while the operating mode functions as an implicit output. By regulating the temperature of the heat source or radiator, one can determine the minimum energy consumption by obtaining the optimal operating mode based on the target water withdrawal. Therefore, the operating modes addressed in this section are confined to passive systems.

To fully realize the potential of the adsorbents in a passive continuous system, we have optimized the operating mode for each adsorbent. Our primary focus is on the time it takes for the cylinder to complete one revolution and the area illuminated by the sun. Figure 3A illustrates the cylinder's clockwise rotation from the red triangle (defined as angle zero). Once the adsorption time $t_{AD}$ has elapsed, angle zeros begin to desorb moisture. After the desorption time $t_{DE}$ has elapsed, angle zero completes an adsorption-desorption cycle, and the cylinder completes one rotation. As a result, our solution parameters can be converted into $t_{AD}$ and $t_{DE}$. Figure 3B illustrates the dynamic profile of the

adsorbent at angle zero and the amount of water withdrawn during the operating time. This information can be determined from the operating parameters and the dynamics of the adsorbent. The final water withdrawal is obtained by integrating the entire cylinder. To fully utilize the sunlight, we aim to extract as much water as possible during the eight hours of daylight (8:00 a.m. to 4:00 p.m.) and optimize the operating mode accordingly. Please refer to STAR Methods for further details on the operating procedure.

Figure 3C presents the optimal operating mode scheme for Bina/FCNT at a fixed operating condition of 30°C and 60% RH. Despite the desorption rate being approximately 17 times higher than the adsorption rate, the ratio of adsorption rate to desorption rate does not follow this pattern. This is because the adsorbent requires time to warm up to the desorption temperature, and therefore, a portion of the desorption time is not utilized for water harvesting. Moreover, the adsorption rates of the samples are related to their initial and final values, as described by the LDF equation. The algorithm automatically identifies the optimal operating interval to maximize water extraction. Figure 3D illustrates the variation in water content of the whole adsorbent under optimum working conditions. A line graph was plotted after intercepting the adsorbent at 0° and 180° (Figure 3E). In the first cycle, the adsorbent at 0° adsorbs significantly more than it desorbs, resulting in the retention of a portion of the water in the adsorbent. The adsorbent with an angle of 180° experienced a shorter first cycle as it underwent only a portion of the adsorption time. It then underwent staggered adsorption/desorption with the adsorbent at 0°. In subsequent cycles, adsorption and desorption gradually stabilize within an interval where all the atmospheric water that has been adsorbed can be converted into liquid water. At any given time, a portion of the adsorbent is in the desorption zone, producing liquid water. Figure S6 shows the results of the other two adsorbents' optimal operating modes. Furthermore, while the optimal operating mode varied under different environmental conditions, the differences were insignificant. Table S2 illustrates the error margin between our selected operating mode and the optimal mode, revealing a maximum difference of ±5 min and a resulting variation of under 3% in maximum water yields.

## Geospatial analysis of the maximum water yield

After establishing the operational mode, it is essential to evaluate how the matching of sorbent and environmental conditions affects the performance of the passive system. The efficiency of SAWH is particularly influenced by real-time local weather conditions. Key parameters include temperature and humidity during the adsorption phase, as well as solar radiation intensity and condensation temperature during desorption, all of which significantly impact water production (Figure S7). Since weather patterns exhibit not only daily fluctuations but also seasonal variations, we must consider these seasonal changes comprehensively.

We implemented restrictions on the amount and intermittency of water collection and took seasonal variations into account when screening absorbents. Specifically, we calculated the minimum seasonal water collection volume and its relative standard deviation (RSD). Based on per capita roof area and water demand in Shanghai, we established thresholds of 0.08 g/g for minimum seasonal water collection volume and 0.5 for RSD (detailed in STAR Methods). If the RSD of the seasonal water harvesting volume exceeds 0.5 and the minimum seasonal water harvesting volume is lower than 0.08 g/g, the material is disqualified, regardless of its annual water harvesting potential. Under these criteria, the material that yields the highest annual water output is considered the most suitable sorbent for the region.

By comparing the SWY per year of sorbents and seasonal screening, we attempted to identify the efficient adsorbent for passive continuous SAWH systems that can be deployed globally. Figure 4A shows the average liquid water collection of the passive system in 2022, assuming no sorbent replacement throughout the year. Figure 4B illustrates the selection of the optimal hygroscopic hydrogel. The SWY ranges from 0 to 2.5 g/g, and about 39.53% of the total land area can stabilize year-round water withdrawals. Regions with the greatest application potential are predominantly high-temperature and high-humidity areas near the equator, particularly in Southeast Asia, Central Africa, and northern South America. In these regions, SMAG is the preferred sorbent. Conversely, LiCl@rGO-SA is a suitable choice for arid areas; however, significant regions marked in light gray do not fulfill the requirements for RSD or minimum water withdrawal. A seasonal comparison of the maps (Figures S8 and S9) reveals that these light gray areas (approximately 40.24% of the land area) pose challenges for water extraction during the winter months. Nonetheless, effective water withdrawal remains attainable in these regions during other seasons. Additionally, regions located above 45° latitude, indicated in dark gray, face limitations in water availability due to insufficient solar irradiation or high elevation, where temperatures can fall below the freezing point of water in certain seasons.

We conducted a correlation analysis to qualitatively analyze the meteorological factors affecting SWY. Considering only the SWY of land capable of obtaining water through SAWH is related to several input meteorological data: temperature, humidity ratio, barometric pressure, and solar irradiation intensity (Figure S10). The results showed that the humidity ratio is the most strongly correlated with the SWY (approximately 86.41%), followed by the temperature and solar radiation (approximately 47.41% and 28.80%), and atmospheric pressure had little correlation with SWY. Both the temperature and humidity ratio exhibit a positive correlation with SWY. In other words, higher temperatures and humidity levels result in increased water harvesting.

## Geospatial analysis of the minimum energy requirements

Figure 5A shows the average minimum energy requirements for the active systems throughout the year, and Figure 5B shows the most suitable hygroscopic hydrogels for each location. The average minimum energy required by the three composite sorbents to harvest 1 kg of water from the atmosphere ranges from 0.3 to 1.4 MJ/kg. The active systems cover 55.27% of the continent, allowing active access to fresh water at all times, greatly exceeding the area suitable for passive systems. High energy demands are concentrated in northern Africa, the Middle East, Australia, northwestern China, and the western United States. These results are consistent with the understanding that

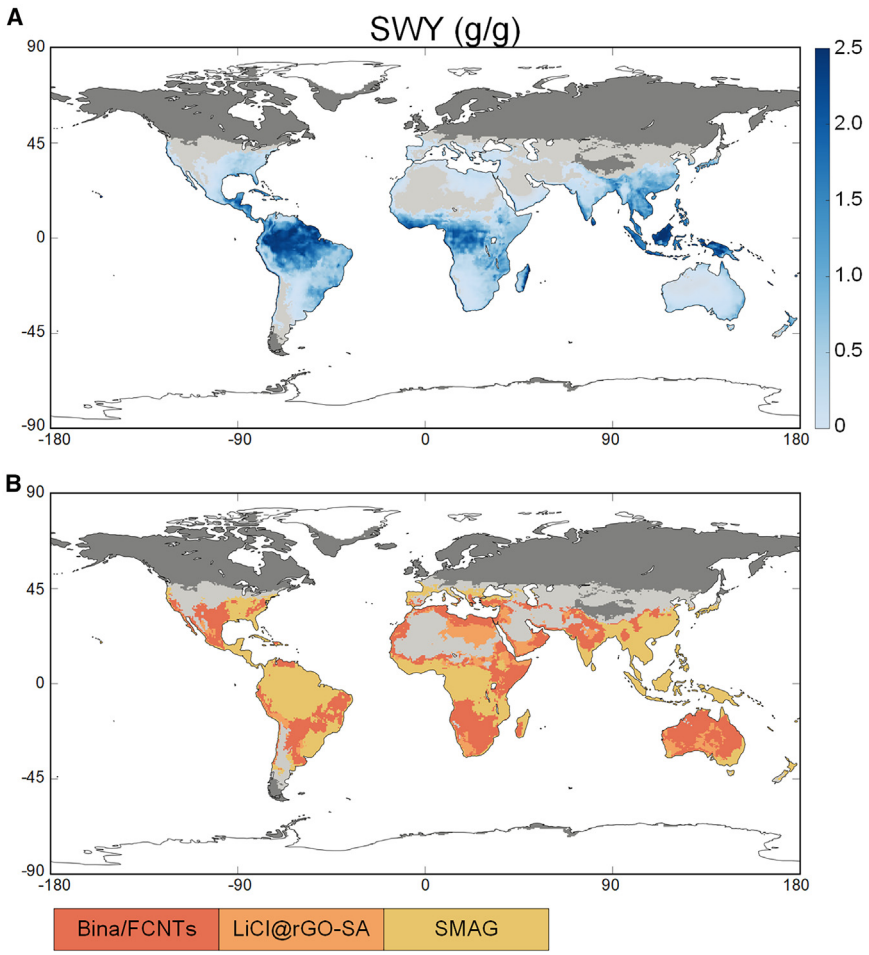


**Figure 4. Optimal SWY distribution map for a solar-driven all-in-one SAWH**

(A) Annual average maximum SWY.

(B) Applicable range of best sorbents for producing liquid water. Uncolored areas are completely unavailable for passive SAWH for the whole year; dark gray areas yield zero water for at least one season (usually in high-latitude or high-altitude areas featuring cold climates); light gray areas cannot yield water evenly or continuously.

water extraction in regions with limited access to water requires more energy. Similar to the modeling of passive systems, we also specify the maximum acceptable energy consumption as well as the RSD for active systems. The results indicate that a small portion of the Sahara Desert, colored in light gray, requires significantly higher energy for effective water extraction. Due to the cooler winter temperatures, it was nearly impossible to apply SAWH to the dark gray shaded areas on the map (detailed in Figures S11 and S12).

Figure 5B shows an intriguing result: Bina/FCNTs can be applied to regions with high energy consumption as well as cold regions with low energy consumption. Because the inputs to the model are all state quantities of air, we conducted calculations based on the enthalpy-moisture diagram to explain this finding. As shown in Figure 5, Bina/FCNTs is the preferred option for both high humidity (RH > 77%) and moderate humidity conditions, whereas SMAG is favorable for all other working conditions. LiCl@rGO-SA is suitable for application in only extremely arid environments, which explains its absence in Figure 5B. It is important to note that previous work has shown that in high humidity areas (>60% RH), the condensation-based AWH approach is a more energy-efficient option than adsorption-based due to the easier attainment of dew point temperatures.[31]

A sensitivity analysis was performed to identify the factors influencing the energy consumption. Figures 6A and 6B show the effect of the temperature and RH on energy consumption. Higher humidity ratio and RH correspond to lower energy consumption. A higher temperature corresponds to higher energy consumption from the viewpoint of the humidity ratio, whereas the opposite is true from the viewpoint of the RH. Figures 6C and 6D highlight the close correlation between the demarcation line for the various adsorbents and RH, which may be related to the shape of the isotherms. The size relationships of the isotherm slope for the three adsorbents were calculated to be LiCl@rGO-SA (<15% RH), Bina/FCNTs (15%–40% RH), SMAG (40%–80% RH), and Bina/FCNTs (>80% RH), which are approximately 5% higher than the cut-offs depicted in the graph. Overall, the effect of the RH must be further investigated, and the temperature and humidity have a limited effect. Although the atmospheric pressure, circulating water yield, heat of adsorption, and specific heat influence the energy consumption, their effect is essentially linear and limited (Figure S13).

## Regional challenge

As discussed in the previous two sections, the performance of absorbents (in terms of water yields and energy consumption) varies across regions worldwide. To examine the effect of the adsorbent on the continuous system performance and select adsorbents based on local considerations, three typical cities or regions spanning the range of climates were selected (Figure S14; Table S3): the Sahara Desert (hot and dry), Beijing (cold and wet), and New Delhi (variable humidity). According to the high-precision weather data recording by hours, the detailed calculation basis of sorbents' daily performances for the three regions was presented in Figures S15–S17, respectively. Each figure shows the local climate, the calculated daily water harvesting, and the energy consumption for each adsorbent.

The Sahara Desert is a typical desert climate with high temperatures and low humidity throughout the year, especially during the summer months. As is shown in Figure S15, although the

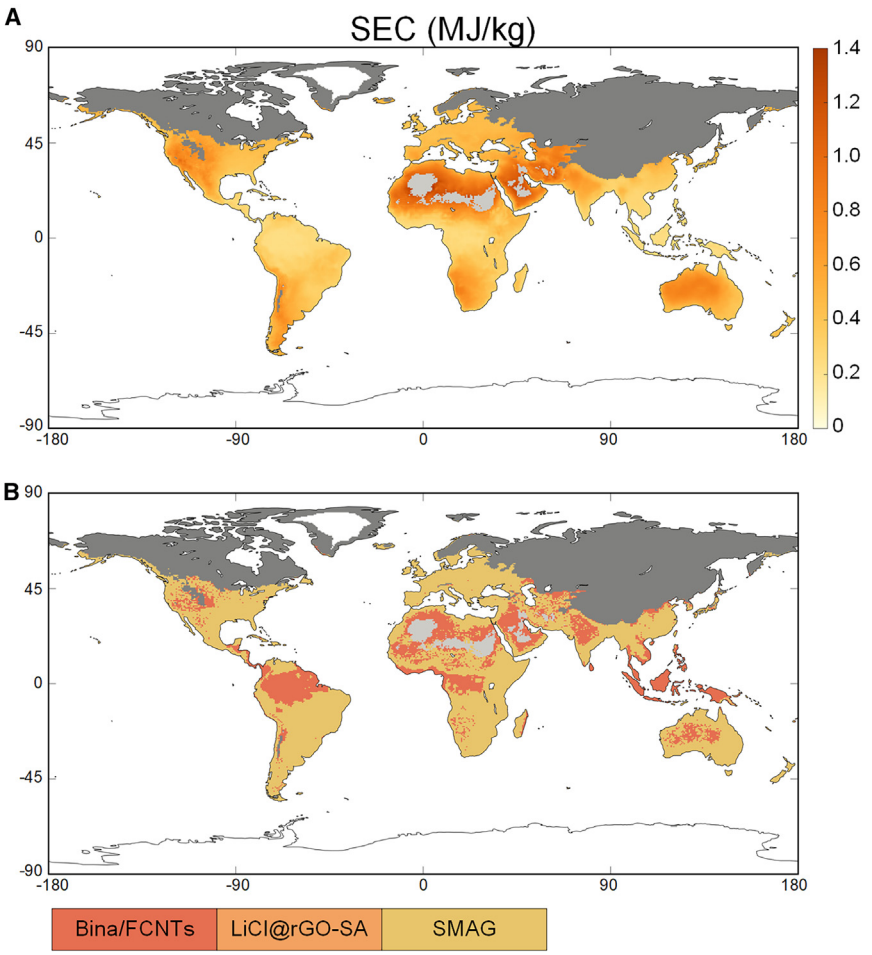


**Figure 5. Optimal SEC distribution for the active SAWH system**

(A) Minimum energy requirements averaged for the year.

(B) Applicable range of the best adsorbents to minimize energy consumption. Uncolored areas are completely unavailable for active SAWH throughout the whole year; dark gray areas cannot harvest water for at least one season of the year; light gray areas represent uneven or discontinuous energy consumption used to harvest water.

desert is abundant in solar resources, it needs to face the dilemma of a low RH of 20% in summer. Therefore, it is important to select adsorbents with inclined isotherms around 20%–30%. LiCl@rGO-SA is not only able to adsorb more water at low RH but also has a fast adsorption rate. However, the maximum water extraction capacity of passive systems in the Sahara Desert is inherently limited. In contrast, active systems demonstrate the potential to significantly enhance water yields when adequate energy is available. To meet daily water demands, it is advisable to integrate one or more active components, such as adsorption radiators, desorption heat sources, or condensation radiators.

Cold regions such as Beijing (Figure S16) may be too cold to apply SAWH in the winter, facing the opposite difficulty to the Sahara Desert. Regarding stability, there are two potential pitfalls in cold regions. The first is the inability to consistently draw water year-round, which can be alleviated with water storage equipment. The second is the significant fluctuations in RH caused by minute changes in humidity ratio at low temperatures, which imposes additional requirements on the operational strategy of the continuous systems during the day, including cycle times and adsorption/desorption ratio.

Figure S17 shows that New Delhi experiences significant seasonal fluctuations, which lead to several interesting results. New Delhi typically experiences three seasons: a cool season (October to March), a hot season (April to June), and a rainy season (July to September). The hot season is similar to the Sahara Desert, where LiCl@rGO-SA is the best adsorbent; while the rainy season is similar to Beijing, where SMAG is more advantageous in high humidity; and the cool season is optimal for Bina/FCNTs. Although Bina/FCNTs are better in all-year comparison, the significant seasonal fluctuations remind us that changing adsorbents according to the seasons by our models, if possible, will lead to performance enhancement of SAWH using in New Delhi.

## DISCUSSION

To address the urgent global need for safe drinking water, particularly in remote areas, it is essential to deploy truly sustainable freshwater harvesting systems. This study develops models of ideal passive and active continuous SAWH systems to evaluate the performance of adsorbents in terms of water harvesting volume and energy demand. Through geospatial analysis using high-precision meteorological data, we assess the potential and feasibility of continuous SAWH systems with different adsorbents across various climatic conditions.

Overall, our findings indicate that adsorbents with higher hygroscopicity, steeper isotherms, and faster kinetics are advantageous for continuous systems under the same climatic conditions. Additionally, temperature and humidity have a more significant impact on system performance than pressure or solar radiation. In regions with high temperatures and humidity, passive systems benefit from enhanced water adsorption, while active systems require less energy for adsorbent regeneration. This research is a valuable resource for optimizing existing sorbents and developing site-specific deployment strategies. It also provides insights for enhancing the performance of continuous SAWH systems through guidelines on novel sorbent preparation, deployment of active components, and operational modes, ultimately contributing to efficient water supply solutions in water-scarce regions worldwide.

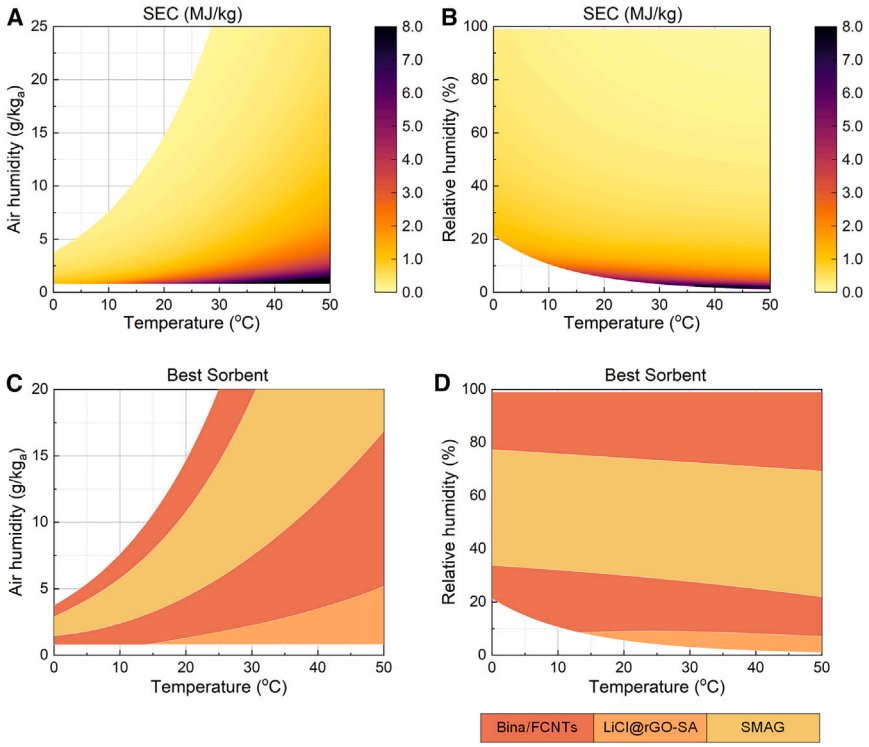


**Figure 6. Sensitivity analysis of active system for temperature and humidity**

(A) Minimum energy consumption for three hygroscopic composite adsorbents on the psychrometric chart.

(B) Variation of minimum energy consumption with temperature and relative humidity.

(C) The applicable range of adsorbents corresponding to achieving the optimal energy requirement.

(D) The most suitable sorbent corresponding to (B). The three dividing lines from bottom to top range roughly from 9%, 29%, and 73% at 25°C.

## Limitations of the study

The first limitation of this study is that local demographic and economic conditions were not considered in the study of different cities. Our maps are based on latitude and longitude and not on district city or region boundaries. However, population, floor space, economic conditions, etc., are based on cities or regions. Future studies can try to break this limitation.

Besides, some assumptions about sorbent modeling, interconnections between water production and energy demand, and passive and active modeling are necessary. We incorporated the more general LDF model in the SAWH and assumed a uniform value for the adsorption kinetic constant k for a given adsorbent in different operating conditions (Figure S1; Table S4). In addition, daily averages were used in the calculations for the active model, and therefore, the value of the circulating water yield had to be smaller than the limit of water uptake in 1 h for the three hydrogels. We set the circulating water yield as 1.5 g/g (Figure S18). The model considered the heat of adsorption and thermal desorption properties of the hygroscopic hydrogels. Notably, the heat of adsorption depends on the operating conditions, as indicated in Figure S19. In addition, the thermal response properties of the gel adsorbent were retained, which means that desorption occurs only when the desorption temperature is more than 55°C. Moreover, in the water yield model, the heat source is the solar collector. Through a thermal conductive substrate, the sorbent is in thermal contact with the solar collector. All of the solar energy is converted to sensible heat through a solar collector for the solar collector, substrate, and sorbent. The efficiency of the solar collector is shown in Figure S20. According to the second-order heat transfer equation, the desorption temperature depends on the local solar radiation intensity and corresponding ambient temperature (detailed in STAR Methods).

## RESOURCE AVAILABILITY

### Lead contact

Further information and requests for resources and reagents should be directed to and will be fulfilled by the lead contact, Jiayun Wang (jywang@usst.edu.cn).

### Materials availability

This study did not generate any new physical materials.

### Data and code availability

- This paper analyzes existing, publicly available data that are listed in the key resources table.
- The code for each process model can be accessed on GitHub upon publication. Accession numbers are listed in the key resources table.
- Any additional information required to reanalyze the data reported in this paper is available from the lead contact upon reasonable request.

## ACKNOWLEDGMENTS

The authors gratefully acknowledge the support and funding for this research sponsored by the General program of the National Natural Science Foundation of China (no. 52376203).

## AUTHOR CONTRIBUTIONS

Conceptualization, W.Y., R.W., and J.W.; methodology, W.Y., C.L., and L.H.; validation, L.Y.; software, W.Y.; writing – original draft, W.Y.; writing – review & editing, W.Y. and C.L.; visualization, W.Y.; supervision, L.Y. and R.W.; project administration, H.Z., R.W., and J.W.; funding acquisition, J.W.

## DECLARATION OF INTERESTS

The authors declare no competing interests.

## STAR★METHODS

Detailed methods are provided in the online version of this paper and include the following:

- KEY RESOURCES TABLE
- METHOD DETAILS
  - Indoor experiment
  - Meteorological data processing
  - Passive system model
  - Minimum energy requirement model
  - Optimization of the continuous system
  - Selection of global map threshold
  - Solar collector parameters
- QUANTIFICATION AND STATISTICAL ANALYSIS

## SUPPLEMENTAL INFORMATION

Supplemental information can be found online at https://doi.org/10.1016/j.isci.2025.112160.

Received: July 8, 2024
Revised: September 29, 2024
Accepted: February 28, 2025
Published: March 5, 2025

## REFERENCES

1. Mekonnen, M.M., and Hoekstra, A.Y. (2016). Four billion people facing severe water scarcity. Sci. Adv. *2*, e1500323. https://doi.org/10.1126/sciadv.1500323.
2. Dinar, A., Tieu, A., and Huynh, H. (2019). Water scarcity impacts on global food production. Glob. Food Sec. *23*, 212–226. https://doi.org/10.1016/j.gfs.2019.07.007.
3. Oki, T., and Kanae, S. (2006). Global hydrological cycles and world water resources. Science *313*, 1068–1072. https://doi.org/10.1126/science.1128845.
4. Dang, C., Cao, Y., Nie, H., Lang, W., Zhang, J., Xu, G., and Zhu, M. (2024). Structure integration and architecture of solar-driven interfacial desalination from miniaturization designs to industrial applications. Nat. Water *2*, 115–126. https://doi.org/10.1038/s44221-024-00200-1.
5. Lei, C., Guan, W., Zhao, Y., and Yu, G. (2024). Chemistries and materials for atmospheric water harvesting. Chem. Soc. Rev. *53*, 7328–7362. https://doi.org/10.1039/d4cs00423j.
6. Jarimi, H., Powell, R., and Riffat, S. (2020). Review of sustainable methods for atmospheric water harvesting. Int. J. Low Carbon Technol. *15*, 253–276. https://doi.org/10.1093/ijlct/ctz072.
7. Gido, B., Friedler, E., and Broday, D.M. (2016). Assessment of atmospheric moisture harvesting by direct cooling. Atmos. Res. *182*, 156–162. https://doi.org/10.1016/j.atmosres.2016.07.029.
8. Woods, J. (2014). Membrane processes for heating, ventilation, and air conditioning. Renew. Sustain. Energy Rev. *33*, 290–304. https://doi.org/10.1016/j.rser.2014.01.092.
9. Bai, Z., Wang, P., Xu, J., Wang, R., and Li, T. (2024). Progress and perspectives of sorption-based atmospheric water harvesting for sustainable water generation: Materials, devices, and systems. Sci. Bull. *69*, 671–687. https://doi.org/10.1016/j.scib.2023.12.018.
10. Xu, W., and Yaghi, O.M. (2020). Metal-Organic Frameworks for Water Harvesting from Air, Anywhere, Anytime. ACS Cent. Sci. *6*, 1348–1354. https://doi.org/10.1021/acscentsci.0c00678.
11. Conde, M.R. (2004). Properties of aqueous solutions of lithium and calcium chlorides: formulations for use in air conditioning equipment design. Int. J. Therm. Sci. *43*, 367–382. https://doi.org/10.1016/j.ijthermalsci.2003.09.003.
12. Kim, K.M., Oh, H.T., Lim, S.J., Ho, K., Park, Y., and Lee, C.H. (2016). Adsorption Equilibria of Water Vapor on Zeolite 3A, Zeolite 13X, and Dealuminated Y Zeolite. J. Chem. Eng. Data *61*, 1547–1554. https://doi.org/10.1021/acs.jced.5b00927.
13. Nguyen, H.L., Gropp, C., Hanikel, N., Möckel, A., Lund, A., and Yaghi, O.M. (2022). Hydrazine-Hydrazide-Linked Covalent Organic Frameworks for Water Harvesting. ACS Cent. Sci. *8*, 926–932. https://doi.org/10.1021/acscentsci.2c00398.
14. Kim, H., Yang, S., Rao, S.R., Narayanan, S., Kapustin, E.A., Furukawa, H., Umans, A.S., Yaghi, O.M., and Wang, E.N. (2017). Water harvesting from air with metal-organic frameworks powered by natural sunlight. Science *356*, 430–434. https://doi.org/10.1126/science.aam8743.
15. Hanikel, N., Prévot, M.S., Fathieh, F., Kapustin, E.A., Lyu, H., Wang, H.Z., Diercks, N.J., Glover, T.G., and Yaghi, O.M. (2019). Rapid Cycling and Exceptional Yield in a Metal-Organic Framework Water Harvester. ACS Cent. Sci. *5*, 1699–1706. https://doi.org/10.1021/acscentsci.9b00745.
16. Rieth, A.J., Yang, S., Wang, E.N., and Dincă, M. (2017). Record Atmospheric Fresh Water Capture and Heat Transfer with a Material Operating at the Water Uptake Reversibility Limit. ACS Cent. Sci. *3*, 668–672. https://doi.org/10.1021/acscentsci.7b00186.
17. Hanikel, N., Pei, X., Chheda, S., Lyu, H., Jeong, W., Sauer, J., Gagliardi, L., and Yaghi, O.M. (2021). Evolution of water structures in metal-organic frameworks for improved atmospheric water harvesting. Science *374*, 454–459. https://doi.org/10.1126/science.abj0890.
18. Alezi, D., Li, R., Alsadun, N., Malik, A., Shekhah, O., Wang, P., and Eddaoudi, M. (2024). Metal-organic framework-based atmospheric water harvesting for enhanced photovoltaic efficiency and sustainability. Mater. Adv. *5*, 4660–4667. https://doi.org/10.1039/d3ma00960b.
19. Entezari, A., Ejeian, M., and Wang, R. (2020). Super Atmospheric Water Harvesting Hydrogel with Alginate Chains Modified with Binary Salts. ACS Mater. Lett. *2*, 471–477. https://doi.org/10.1021/acsmaterialslett.9b00315.
20. Xu, J., Li, T., Yan, T., Wu, S., Wu, M., Chao, J., Huo, X., Wang, P., and Wang, R. (2021). Ultrahigh solar-driven atmospheric water production enabled by scalable rapid-cycling water harvester with vertically aligned nanocomposite sorbent. Energy Environ. Sci. *14*, 5979–5994. https://doi.org/10.1039/d1ee01723c.
21. Deng, F., Chen, Z., Wang, C., Xiang, C., Poredoš, P., and Wang, R. (2022). Hygroscopic Porous Polymer for Sorption-Based Atmospheric Water Harvesting. Adv. Sci. *9*, e2204724. https://doi.org/10.1002/advs.202204724.
22. Zhao, F., Zhou, X., Liu, Y., Shi, Y., Dai, Y., and Yu, G. (2019). Super Moisture-Absorbent Gels for All-Weather Atmospheric Water Harvesting. Adv. Mater. *31*, 1806446. https://doi.org/10.1002/adma.201806446.
23. Xiang, C., Yang, X., Deng, F., Chen, Z., and Wang, R. (2023). Daytime air–water harvesting based on super hygroscopic porous gels with simultaneous adsorption–desorption. Appl. Phys. Rev. *10*, 041413. https://doi.org/10.1063/5.0160682.
24. Shan, H., Zeng, Z., Yang, X., Poredoš, P., Yu, J., Chen, Z., and Wang, R. (2023). Harvesting Thermal Energy and Freshwater from Air through Sorption Thermal Battery Enabled by Polyzwitterionic Gel. ACS Energy Lett. *8*, 5184–5191. https://doi.org/10.1021/acsenergylett.3c01836.
25. Poredos, P., Shan, H., Wang, C.X., Deng, F.F., and Wang, R.Z. (2022). Sustainable water generation: grand challenges in continuous atmospheric water harvesting. Energy Environ. Sci. *15*, 3223–3235. https://doi.org/10.1039/d2ee01234k.
26. LaPotin, A., Zhong, Y., Zhang, L., Zhao, L., Leroy, A., Kim, H., Rao, S.R., and Wang, E.N. (2021). Dual-Stage Atmospheric Water Harvesting Device

for Scalable Solar-Driven Water Production. Joule *5*, 166–182. https://doi.org/10.1016/j.joule.2020.09.008.

27. Li, C., Pan, Q., Ying, W., Shan, H., Wang, R., Zhang, H., and Wang, J. (2022). Atmospheric water harvesting with scale-up potentials using natural sunlight and passive cooling. Nat. Sci. *3*, e20220038. https://doi.org/10.1002/ntls.20220038.
28. Li, R., Shi, Y., Wu, M., Hong, S., and Wang, P. (2020). Improving atmospheric water production yield: Enabling multiple water harvesting cycles with nano sorbent. Nano Energy *67*, 104255. https://doi.org/10.1016/j.nanoen.2019.104255.
29. Poredos, P., and Wang, R.Z. (2023). Sustainable cooling with water generation. Science *380*, 458–459. https://doi.org/10.1126/science.add1795.
30. Kim, H., Rao, S.R., LaPotin, A., Lee, S., and Wang, E.N. (2020). Thermodynamic analysis and optimization of adsorption-based atmospheric water harvesting. Int. J. Heat Mass Transf. *161*, 120253. https://doi.org/10.1016/j.ijheatmasstransfer.2020.120253.
31. Hua, L., Xu, J., and Wang, R. (2021). Exergy-efficient boundary and design guidelines for atmospheric water harvesters with nano-porous sorbents. Nano Energy *85*, 105977. https://doi.org/10.1016/j.nanoen.2021.105977.
32. Feng, Y., Wang, R., and Ge, T. (2022). Pathways to Energy-efficient Water Production from the Atmosphere. Adv. Sci. *9*, e2204508. https://doi.org/10.1002/advs.202204508.
33. Lord, J., Thomas, A., Treat, N., Forkin, M., Bain, R., Dulac, P., Behroozi, C.H., Mamutov, T., Fongheiser, J., Kobilansky, N., et al. (2021). Global potential for harvesting drinking water from air using solar energy. Nature *598*, 611–617. https://doi.org/10.1038/s41586-021-03900-w.
34. Kocher, J.D., and Menon, A.K. (2023). Addressing global water stress using desalination and atmospheric water harvesting: a thermodynamic and technoeconomic perspective. Energy Environ. Sci. *16*, 4983–4993. https://doi.org/10.1039/d3ee02916f.
35. Rao, A.K., Fix, A.J., Yang, Y.C., and Warsinger, D.M. (2022). Thermodynamic limits of atmospheric water harvesting. Energy Environ. Sci. *15*, 4025–4037. https://doi.org/10.1039/d2ee01071b.
36. Thommes, M., Kaneko, K., Neimark, A.V., Olivier, J.P., Rodriguez-Reinoso, F., Rouquerol, J., and Sing, K.S. (2015). Physisorption of gases, with special reference to the evaluation of surface area and pore size distribution (IUPAC Technical Report). Pure Appl. Chem. *87*, 1051–1069. https://doi.org/10.1515/pac-2014-1117.
37. Zheng, X., Ge, T.S., Hu, L.M., and Wang, R.Z. (2015). Development and Characterization of Mesoporous Silicate-LiCl Composite Desiccants for Solid Desiccant Cooling Systems. Ind. Eng. Chem. Res. *54*, 2966–2973. https://doi.org/10.1021/ie504948j.
38. Yao, H., Zhang, P., Huang, Y., Cheng, H., Li, C., and Qu, L. (2020). Highly Efficient Clean Water Production from Contaminated Air with a Wide Humidity Range. Adv. Mater. *32*, 1905875. https://doi.org/10.1002/adma.201905875.
39. Yang, K., Pan, T., Pinnau, I., Shi, Z., and Han, Y. (2020). Simultaneous generation of atmospheric water and electricity using a hygroscopic aerogel with fast sorption kinetics. Nano Energy *78*, 105326. https://doi.org/10.1016/j.nanoen.2020.105326.
40. Kim, S., Liang, Y., Kang, S., and Choi, H. (2021). Solar-assisted smart nanofibrous membranes for atmospheric water harvesting. Chem. Eng. J. *425*, 131601. https://doi.org/10.1016/j.cej.2021.131601.
41. Díaz-Marín, C.D., Zhang, L., Lu, Z., Alshrah, M., Grossman, J.C., and Wang, E.N. (2022). Kinetics of Sorption in Hygroscopic Hydrogels. Nano Lett. *22*, 1100–1107. https://doi.org/10.1021/acs.nanolett.1c04216.
42. Wang, J., Deng, C., Zhong, G., Ying, W., Li, C., Wang, S., Liu, Y., Wang, R., and Zhang, H. (2022). High-yield and scalable water harvesting of honeycomb hygroscopic polymer driven by natural sunlight. Cell Rep. Phys. Sci. *3*, 100954. https://doi.org/10.1016/j.xcrp.2022.100954.
43. Global Modeling and Assimilation Office (GMAO) (2015). MERRA-2 statD_2d_slv_Nx: 2d, Daily, Aggregated Statistics, Single-Level, Assimilation, Single-Level Diagnostics V5.12.4 (Greenbelt, MD, USA: Goddard Earth Sciences Data and Information Services Center (GES DISC)). https://doi.org/10.5067/9SC1VNTWGWV3.

## STAR★METHODS

### KEY RESOURCES TABLE

| REAGENT or RESOURCE | SOURCE | IDENTIFIER |
|---|---|---|
| Deposited data | | |
| MERRA-2 statD_2d_slv_Nx: 2d, Daily, Aggregated Statistics, Single-Level, Assimilation, Single-Level Diagnostics V5.12.4 | NASA Global Modeling and Assimilation Office (GMAO) | https://disc.gsfc.nasa.gov/datasets |
| Software and algorithms | | |
| Matlab R2021a | MathWorks | https://www.mathworks.com |
| Global potential analysis code | This work | https://github.com/SAWH-Ying/Continuous-SAWH-pre |

### METHOD DETAILS

#### Indoor experiment

Based on the physical model we developed, we designed an approximate continuous device. The design is identical to the structure in Figure 2A of the manuscript, with the exception of an additional support structure in the adsorption section, as shown in Figure S2. To simulate an outdoor experiment, the device was placed under simulated sunlight.

Figure S3 shows the results of the water harvesting, with most of the droplets concentrated on the copper condensation wall surface rather than the clear glass plate above. Moreover, the bottom of the copper plate is designed with grooves to collect the droplets that are aggregated and then dropped by gravity.

Based on the experimental results, we have defined the heat and mass transfer of adsorption and desorption. As is shown in Figure S5, during the initial 40 minutes of operation, the temperatures of all components gradually increase from ambient temperature, a process commonly referred to as 'warm-up'. Subsequently, the temperature of the entire unit approaches equilibrium and stabilizes over the next 30 minutes. The adsorbent releases heat during adsorption, which raises its temperature by approximately 3°C above ambient. The desorption process accounts for a quarter of the total mass and reduces the temperature by 9°C accordingly. The condensation temperature is maintained at ambient temperature plus 18°C. In the past 30 minutes, our two temperature measurement points exchanged adsorption and desorption states. Both points changed temperature at a rate of 4°C per minute until they reached the adsorption/desorption temperature.

#### Meteorological data processing

The raw meteorological data included daily hourly time-averaged and two-dimensional data for 2022, with a spatial resolution of 0.625 ° × 0.5 °. These data were extracted from the NASA Modern-Era Retrospective Analysis for Research and Applications, version 2 project.[43] This ensemble consisted of the atmospheric temperature at the surface, humidity, surface pressure, and incoming shortwave flux (i.e., solar radiation).

The formulation of $RH$ regarded to the material temperature $T$, air inlet humidity $\omega_a$ and atmospheric pressure $P_{atm}$ is shown below.

$$\begin{cases} P_{sat} = exp\left(\frac{C_1}{T} + C_2 + C_3 T + C_4 T^2 + C_5 T^3 + C_6\, ln(T)\right) * 6890 \\ RH = \frac{P_{atm}}{P_{sat}} \frac{1}{\frac{0.621945}{\omega_a} + 1} \end{cases} \quad \text{(Equation 1)}$$

where $P_{sat}$ denotes the saturation pressure of water vapor at temperature $T$ in pa. The coefficients $C$ are -1.0440397E+4, -1.129465E+1, -2.7022325E-2, 1.289036E-5, -2.4780681E-9, and 6.5459673E+1 respectively. T denotes the temperature in °R, which is converted to Rankine temperature by the formula [°R] = [°C]*9/5+32+459.67 or [°R] = [K]*9/5. $P_{atm}$ denotes the atmospheric pressure in pa, and $\omega_a$ denotes the humidity ratio in g/kga. The meaning of all the symbols in manuscript can be found in Table S5.

#### Passive system model

For passive SAWH device, the final amount of liquid water obtained $\Delta W$ is the difference between the amount of moisture absorbed by the sorbent during adsorption and desorption.

$$\Delta W = W_{AD} - W_{DE} \quad \text{(Equation 2)}$$

Where $W_{AD}$ and $W_{DE}$ represent the equilibrium moisture contents of the adsorbent at the completion of adsorption and desorption processes, respectively. Under ideal conditions with sufficient adsorption/desorption duration, the adsorption amount is a function of the environmental conditions (temperature, humidity) and the adsorbent isotherm (Equation 3).

$$W_{max} = W_s^{\omega}(\omega_s, T_s) \quad \text{(Equation 3)}$$

Where $W_{max}$ is the equilibrium moisture content in the given operating conditions, obtained from the isotherm. $T_s$ and $\omega_s$ denote the temperature and humidity ratio of the air near the adsorbent, respectively. The relative humidity of the air can be calculated by empirical formula and the maximum water uptake of the adsorbent can be determined by isotherms.

However, when kinetic limitations are considered, a comprehensive analysis requires the integration of both thermodynamic and kinetic models to accurately determine the transient adsorption state of the adsorbent. The classical linear driven force equation is used to represent the adsorption kinetics of the sorbent (Equation 4).

$$\frac{\partial W}{\partial t} = k(W_{max} - W) \quad \text{(Equation 4)}$$

Where $k$ denotes kinetics parameter, which can be fitted from adsorption kinetic curve. As shown in Figure 1 in the manuscript, $W_{AD}$ can be obtained by substituting the saturation adsorption amount $W_{AD,max}$, the adsorption rate $k_{AD}$ and the adsorption time $t_{AD}$. The saturation adsorption capacity is obtained from the adsorption temperature $T_{s,AD}$ and the ambient humidity $\omega_{amb}$. Meanwhile, for passive systems without adsorption cooling source, the heat of adsorption released by adsorption can be considered to be carried away by the environment and therefore the adsorption temperature is approximated by the ambient temperature $T_{amb}$. If the analytic form of the isotherms is denoted as $W^{\omega}{}_d(\omega_a, T_d)$, the $W_{AD}$ can then be represented as Equation 5.

$$\begin{cases} W_{AD} = (1 - \exp(-k_{AD}t_{AD}))(W_{AD,max} - W_{AD,ini}) + W_{AD,max} \\ W_{AD,max} = W_s^{\omega}(\omega_{amb}, T_{AD}), T_{AD} = T_{amb} + 3 \end{cases} \quad \text{(Equation 5)}$$

Here, we present the process to derive the exact formulation of $W^{\omega}{}_s(\omega_a, T_d)$. The formulation of $W^{\omega}{}_s$ can be rearranged by a theorem in literature claims that, the adsorption water content $W_s$ is, to some degree, a one-variable function of adsorption potential $\Delta F$, while $\Delta F$ is analytically correlated with material temperature $T_d$ and material relative humidity $RH_s$. The mathematical expression of the theorem is presented as below Equation 6.

$$\begin{cases} W_{AD,max} = W_s^{\omega}(\omega_a, T_d) = W_s^{\Delta F}\left(\Delta F_s^{RH}(RH_s, T_s)\right) = W_s^{RH}(RH_s(\omega_a, T_s), T_s) \\ \Delta F_s^{RH}(RH_s, T_s) = -\dfrac{RT_s\, ln(RH_s)}{M_w} \end{cases} \quad \text{(Equation 6)}$$

Where: $R$ is the gas constant, the value is 8.314J/mol/K, $M_w$ is the molar mass of water, the value is 18 g/mol, $T$ and $RH$ are the adsorbent surface temperature ($K$) and relative humidity (%), respectively. Only when the material temperature and humidity are respectively equal to the ambient temperature and humidity, $RH_s$ is equivalent to the ambient relative humidity. Based on the above analysis, the essence of Equation 6 can be regarded as the variable substitution from $\omega_a$ to $RH_s$.

Analytic formulation of $W^{RH}{}_s(RH_s, T_s)$ is not easily accessible in literature, especially for new materials. However, experimental sorption isotherms under specific temperatures (normally from 20-30°C for adsorption) are abundant for composite sorbents. Namely, the tabular relationship of $W^{RH}{}_s(RH_s, T_s)$ during the adsorption phase under a reference temperature $T_{ADref}$ are available, denoted as $W^{RH}{}_{ADref}(RH_s, T_{ADref})$. Then, based on the theorem in Equation 6, we can generalize the formulation of $W^{RH}{}_{ADref}$ at the reference temperature to $W^{RH}{}_s(RH_s, T_s)$ at arbitrary temperature by introducing an equivalent relative humidity (Equation 7). The detailed derivation is shown in Equation 8.

$$RH'_{AD} = \exp\left(\frac{T_s}{T_{ADref}}\ln(RH_s)\right) \quad \text{(Equation 7)}$$

$$\begin{aligned} W_s^{RH}(RH_s, T_s) &= W_s^{\Delta F}\left(-\frac{RT_s\, ln(RH_s)}{M_w}\right) \\ &= W_s^{\Delta F}\left(-\frac{RT_{ADref}\, ln\left(RH'_{AD}\right)}{M_w}\right) \\ &= W_{ADref}^{RH}\left(RH'_{AD}, T_{ADref}\right) \end{aligned} \quad \text{(Equation 8)}$$

For desorption process, $W_{DE,max}$ can be ascertained by the isotherm of the specific sorbent corresponding to the desorption temperature $T_{s,DE}$ along with the air humidity at the desorption bed inlet $\omega_{ai,DE}$ (when desorption is completed). As shown in Figure 2C, the air inlet humidity of the desorption bed is the same as the air outlet humidity of the condenser, namely, the saturated wet air at

condensing temperature ($\omega_{CD}$=$\omega_{ai,DE}$). We assume a condenser with no heat source but finite convective heat transfer coefficient, which typically results in a condensing temperature 5°C to 10°C higher than the ambient temperature.[12] for a fair comparison, we uniformly choose 8°C as their difference. For this assumption

$$W_{DE} = W_s^{\omega}(\omega_{ai,DE}, T_{DE}, k_{DE}, t_{DE}) \quad \text{(Equation 9)}$$

$$T_{CD} = T_{amb} + 16 \quad \text{(Equation 10)}$$

$$\omega_{ai,DE} = \omega_{ao,CD} = 0.621945\left(\frac{P_{sat}(T_{CD})}{P_{atm}} - 1\right) \quad \text{(Equation 11)}$$

Since we use solar collector panels in passive SAWH installations, the desorption temperature $T_{ao,DE}$ is determined by the solar irradiation intensity $SR_{amb}$ and the ambient temperature $T_{amb}$. This relationship is described in more detail in Equation 38.

$$T_{d,DE} = f(SR_{amb}) + T_{amb} - 9 \quad \text{(Equation 12)}$$

According to Equations 6, 7, and 8, we can likewise obtain the exact amount of water remaining in the sorbent at the end of desorption, in the virtue of the tabular relationship of $W^{RH}{}_s(RH_s, T_s)$ during the desorption phase under a reference temperature $T_{DEref}$, denoted as $W^{RH}{}_{DEref}(RH_s, T_{DEref})$. Here, $RH_s$ is the function of material temperature $T_{s,DE}$ and inlet air humidity $\omega_{ai,DE}$.

$$\begin{cases} RH'_{DE} = \exp\left(\dfrac{T_s}{T_{DEref}}\ln(RH_s)\right) \\ W_s^{\omega}(\omega_a, T_s) = W_s^{RH}(RH_s, T_s) = W_{DEref}^{RH}(RH'_{DE}, T_{DEref}) \end{cases} \quad \text{(Equation 13)}$$

Where the isotherm of desorption is usually measured at 55°C ~85°C, and the reference temperature of desorption $T_{ref}$ is taken as 70°C.And the general flow chart is shown in Figure S21.

## Minimum energy requirement model

As it is mentioned in the manuscript, in active SAWH systems, three temperature sources (at most) can be employed, to respectively provide cooling or heating energy for adsorption (cooling), desorption (heating) and also condensation (cooling). However, manipulating the temperature will consume active energy like electricity. An appropriate performance index for an active system might be the ratio between the input and output, that is, the specific energy consumption (*SEC*) to establish the energy source under the current ambient conditions per unit water yield. This section elucidates the thermodynamic model of *SEC* evaluation under the specific weather condition ($T_{amb}$, $\omega_{amb}$). For a fair comparison, we set all sorbents to be calculated at the same specific water yield per sorbent mass per cycle $\Delta W$ and the same specific water harvesting rate per air flow rate $\Delta\omega_{rate}$. Namely, the energy consumption of active systems with different sorbents are compared based on the same amount of material, input air flow rate and water yield.

We assume, at first, the source temperature for adsorption, desorption and condensation respectively as ($T_{s,AD}$, $T_{s,DE}$, $T_{s,CD}$). Then, the operational conditions of the adsorbent and the air can be represented analytically as functions of the source temperature and the transient weather condition: $f(T_{s,AD}, T_{s,DE}, T_{s,CD}, T_{amb}, \omega_{amb})$. The overall consumed energy, water yield and specific energy consumption (*SEC*) can then be derived from the operational conditions, also in the form of $f(T_{s,AD}, T_{s,DE}, T_{s,CD}, T_{amb}, \omega_{amb})$. Finally, the criterion of *SEC* can be minimized via exhausting all the possible combination of source temperatures ($T_{s,AD}$, $T_{s,DE}$, $T_{s,CD}$) for each material. This minimization, in turns, determines the optimal source temperatures, denoted as ($T^*_{s,AD}$, $T^*_{s,DE}$, $T^*_{s,CD}$). Detailed processes are presented as below.

### *Adsorption phase*

The calculation of $W_{AD}$ is similar to that of the passive device (Equation 5), but the temperature of the adsorbent is changed into the temperature of the heat source $T_{s,AD}$. In addition, the duration and rate of adsorption do not have to be considered in active installations.

$$W_{AD} = W_s^{\omega}(\omega_{amb}, T_{s,AD}) \quad \text{(Equation 14)}$$

The inlet air comes from the ambient (state I: $T_{ai,AD}$=$T_{amb}$, $\omega_{ai,AD}$=$\omega_{amb}$), while the outlet air from the sorption bed undergoes mass and heat transfer with the sorbent. Specifically, the humidity of the outlet air varies from $\omega^L{}_{a,AD}$ to $\omega^H{}_{a,AD}$ through the course of adsorption, as shown in Figure S2, then an average adsorption state can be approximated according to LDF model (converting the product of adsorption rate and duration into a constant) and Equation 17. Notably, $\omega_a(W_s, T_s)$ in Equation 17 denotes the inverse function of $W_s(\omega_a, T_s)$. The outlet temperature can be deduced from (Equation 18), as previously verified in an article where empirical formulas are given.

$$T_{d,AD} = T_{s,AD} + \Delta T_{AD}, \Delta T_{AD} = 4°C + 1°C\frac{\Delta\omega_{rate}}{5g/kga} \quad \text{(Equation 15)}$$

$$\overline{\omega}_{ao,AD} = \overline{\omega}_{d,AD} - \Delta\omega_{AD}, \Delta\omega_{DE} = 0.2\Delta\omega_{rate} \quad \text{(Equation 16)}$$

$$\overline{\omega}_{d,AD} = \frac{\int_{W_{DE}}^{W_{AD}} \omega_s(W_{d,AD}, T_{d,AD}) dW_{d,AD}}{W_{AD} - W_{DE}}, \omega_a(W_d, T_d) = W_d^{-1}(\omega_a, T_d) \quad \text{(Equation 17)}$$

$$T_{ao,AD} = \min\left(T_{ai,AD} - \eta_{T,AD}(T_{d,AD} - T_{ai,AD}), T_{ai,AD}\right), \eta_{T,AD} = \frac{0.8}{(G_{AD}/G_{DE})^{0.2}} \quad \text{(Equation 18)}$$

### Condensation phase

Provided the condensation temperature of $T_{s,CD}$, the outlet air condition of condensation (state V) can be directly ascertained as shown in Equations 19 and 20, since the condenser cools the air down to its saturated state at the corresponding temperature $T_{s,CD}$.

cools the air down to its saturated state at the corresponding temperature $T_{s,CD}$.

$$T_{ao,CD} = T_{s,CD} + \Delta T_{CD}, \Delta T_{CD} = 4^{\circ}C + 1^{\circ}C\frac{\Delta\omega_{rate}}{5g/kga} \quad \text{(Equation 19)}$$

$$\omega_{ao,CD} = 0.621945\left(\frac{P_{sat}(T_{ao,CD})}{P_{atm}} - 1\right) \quad \text{(Equation 20)}$$

### Desorption phase

The outlet air of the condenser is the inlet condition of the sorption bed during the desorption phase ($T_{ai,DE}$=$T_{ao,CD}$, $\omega_{ai,AD}$=$\omega_{ao,CD}$). Under the assumption of complete desorption and negligible potential difference, the water content after desorption $W_{DE}$ can then be determined by the isotherm corresponding to the employed sorbents under the temperature of $T_{s,DE}$ as shown in Equation 21. However, in this section, the desorption is not necessarily complete. Instead, the end point of desorption is ascertained by a pre-defined specific water yield $\Delta W$. Meanwhile, Equation 21 functions as a constraint since it defines the limitation of the desorption end point under the specific desorption and condensation temperatures, detailed in Equation 22. The overall consequence of Equations 20, 21, and 22 is a constraint imposed on the condensation temperature in this system.

$$W_{DE}^{limit} = W_s(\omega_{ao,CD}, T_{s,DE}) \quad \text{(Equation 21)}$$

$$W_{DE}^{limit} \leq W_{DE} = W_{AD} - \Delta W \quad \text{(Equation 22)}$$

Equations 23 and 24 shows the outlet air from the sorption bed undergoes heat and mass transfer with the sorbent, respectively. Specifically, the humidity of the outlet air varies from $\omega^H_{s,DE}$ to $\omega^L_{s,DE}$ through the course of desorption, as shown in Figure S2, then similar to Equation 15, an average adsorption state can be approximated according to Equation 25. Notably, $\omega_a(W_s, T_s)$ in Equation 25 denotes the inverse function of $W_s(\omega_a, T_s)$. The outlet temperature can be deduced from (Equation 26), as previously verified in an article where empirical formulas are given.

$$T_{d,DE} = T_{s,DE} + \Delta T_{DE}, \Delta T_{DE} = 6^{\circ}C + 1^{\circ}C\frac{\Delta\omega_{rate}}{5g/kga} \quad \text{(Equation 23)}$$

$$\overline{\omega}_{ao,DE} = \overline{\omega}_{d,DE} - \Delta\omega_{DE}, \Delta\omega_{DE} = 0.4\Delta\omega_{rate} \quad \text{(Equation 24)}$$

$$\overline{\omega}_{d,DE} = \frac{\int_{W_{DE}}^{W_{AD}} \omega_a(W_{d,DE}, T_{d,DE}) dW_{d,DE}}{W_{AD} - W_{DE}}, \omega_a(W_d, T_d) = W_d^{-1}(\omega_a, T_d) \quad \text{(Equation 25)}$$

$$T_{ao,DE} = \max(\eta_{T,DE}(T_{d,DE} - T_{ai,DE}) + T_{ai,DE}, T_{ai,DE}), \eta_{T,DE} = 0.8 \quad \text{(Equation 26)}$$

### Energy consumption

In the above processes, thermal energy is extracted/released from the heat source/sinks to overcome the sensible heat of the sorbent, the heat of adsorption and the sensible heat of air, which is summarized in Equation 27.

$$\begin{cases} \dot{Q}_{AD} = \dot{m}_{AD}\left(h^*_{ai,AD} - h^*_{ao,AD}\right) + m_d c_{p,d}(T_{d,DE} - T_{d,AD}) \\ \dot{Q}_{DE} = \dot{m}_{DE}\left(h^*_{ao,DE} - h^*_{ai,DE}\right) + m_d c_{p,d}(T_{d,DE} - T_{d,AD}) \\ \dot{Q}_{CD} = \dot{m}_{DE}(h_{ai,CD} - h_{ao,CD}) \\ m_s = \dfrac{\Delta\omega_{rate}\dot{m}_{DE}}{\Delta W} \\ h_a = c_{pa}T_a + \omega_a\left(c_{pv}T_a + h_{fg}\right), h^*_a = c_{pa}T_a + \omega_a(c_{pv}T_a + q_{st}) \end{cases} \quad \text{(Equation 27)}$$

The heat of adsorption can be calculated by Clausius-Clapeyron equation.

$$lnp = \frac{q_{st}}{RT} + X \quad \text{(Equation 28)}$$

where $p$ is the partial pressure of water vapor and $X$ is the integration constant. It can be noticed from the graphs that the heat of adsorption is all slightly greater than the latent heat of vaporization of water, indicating that for composite adsorbents most of the heat of adsorption comes from the heat of phase change of water.

Particularly, since adsorption dynamics are deemed as main obstacles, a larger flow rate (Equation 29) is adopted to accelerate the process.

$$\frac{\dot{m}_{AD}}{\dot{m}_{DE}} = \max\left(2, \left|\frac{\overline{\omega}_{d,DE} - \omega_{ai,DE}}{\overline{\omega}_{d,AD} - \omega_{ai,AD}}\right|\right) \quad \text{(Equation 29)}$$

The thermal energy extracted/released from the heating source/sinks are not necessarily equal to the consumed electricity or other active energy input. Based on the thermodynamics, it is always more energy-intensive to establish a heat source with higher temperature but the same heat flux. In order to comprehensively evaluate the quantity and quality of energy, the concept of exergy, expressing the "minimum work required to maintain such a heat source/sink", was adopted as a unifying criterion (Equation 30).

$$\begin{cases} \dot{E}x_{AD} = \dfrac{\dot{Q}_{AD}(T_{amb} - T_{d,AD})}{T_{d,AD}} \\ \dot{E}x_{DE} = \dfrac{\dot{Q}_{DE}(T_{d,DE} - T_{amb})}{T_{d,DE}} \\ \dot{E}x_{CD} = \dfrac{\dot{Q}_{CD}(T_{amb} - T_{d,CD})}{T_{d,CD}} \end{cases} \quad \text{(Equation 30)}$$

### Water yield

Based on the definition, specific water harvesting rate (*SWHR*) $\Delta\omega_{rate}$ can be obtained from Equation 31.

$$\Delta\omega_{rate} = \overline{\omega}_{ao,DE} - \omega_{ai,DE} = \overline{\omega}_{d,DE} - \omega_{ao,CD} \quad \text{(Equation 31)}$$

### Specific energy consumption

Equation 32 derives an expression for the *SEC* based on the active SAWH system.

$$SEC = \frac{\dot{E}x_{AD} + \dot{E}x_{DE} + \dot{E}x_{CD}}{\Delta\omega_{rate}\dot{m}_{DE}} \quad \text{(Equation 32)}$$

Finally, the criterion of *SEC* can be minimized via exhausting all the possible combination of source temperatures ($T_{s,AD}$, $T_{s,DE}$, $T_{s,CD}$) for each material. Apart from Equations 14, 15, 16, 17, 18, 19, 20, 21, 22, 23, 24, 25, 26, and 27, some practical constraints are imperative. On the one hand, the temperature of the heat sink should be greater than -5°C to prevent condensation and the temperature of the heat source should not exceed 100°C to prevent overheating. On the other hand, a mediate *SWHR* of 8g/kga is

adopted for all adsorbents. This minimization, in turns, determines the optimal source temperatures, denoted as ($T^*_{s,AD}$, $T^*_{s,DE}$, $T^*_{s,CD}$) as in Equation 33.

$$\begin{cases} \left\{T^*_{s,AD}, T^*_{s,DE}, T^*_{s,CD}\right\} = argmin\left\{SEC, s.t.\left\{\begin{array}{c} SWHR(T_{s,AD}, T_{s,DE}, T_{s,CD}) = 8kg/kga \\ T_{s,AD}, T_{s,CD} \in (-5^\circ C, T_{amb}) \\ T_{s,DE} \in (T_{amb}, 100^\circ C) \end{array}\right\}\right. \\ SEC^* = SEC\left(T^*_{s,AD}, T^*_{s,DE}, T^*_{s,CD}\right) \end{cases} \quad \text{(Equation 33)}$$

And the general flow chart is as Figure S22.

## Optimization of the continuous system

The sorbent undergoes multiple sorption and desorption cycles throughout the day. In order to maximize the performance of continuous device, there are two aspects need to be considered: cycle time and adsorption/desorption ratio. In other words, in this optimization model, there are two decision variables adsorption duration $t_{AD}$ and desorption duration $t_{DE}$. The objective function is maximizing the specific water harvesting throughout the daytime using solar radiation.

$$\max SWY = \frac{8 \cdot 60}{t_{AD} + t_{DE}} \cdot (W_{AD}(t_{AD}) - W_{DE}(t_{DE})) \quad \text{(Equation 34)}$$

where, $W_{AD}(t_{AD})$ is concentration of water in the sorbent after $t_{AD}$ from zero. $W_{DE}(t_{DE})$ is concentration of water in the sorbent after $t_{DE}$ from $t_{AD}$.

In the main program, as is shown in Figure S23, the adsorption duration $t_{AD}$ and desorption duration $t_{DE}$ are varied to calculate the maximum water yields. Assuming that the initial water uptake of the adsorbent is 1.5g/g and the fixation time step is one minute, we calculate the water uptake of the adsorbent per minutes. By comparing the cumulative amount of water desorbed by each adsorbent, we can find the optimal adsorption duration $t_{AD}$ and desorption duration $t_{DE}$.

In this structure, the gray part of the flowchart can be solved for every unit. Firstly, judge whether the unit is in the adsorption or desorption state and then judge its temperature. If the temperature of the unit dose not reach the adsorption or desorption temperature, it will change the temperature forwards to the aimed temperature at a rate of 4°C per minute. Then the water uptake in this moment can be calculated. If this unit is in desorption state, and the water uptake decreased will be condensed to liquid water. Accumulating the liquid water, we obtain the water yields.

## Selection of global map threshold

Real-life water consumption cannot be simplified to an annual basis. Thus, in the selection of sorbents, minimum monthly water yields and its relative standard deviation (RSD) or coefficient of variation (CV) should be considered to reflect the fluctuation throughout the year.

According to the National Academies of Sciences, Engineering, and Medicine, each person needs to intake about 4 L of fresh water per day (specifically 3.7 L for men and 2.7 L for women), within which around 30% is available through the daily diet. The remaining 2.8 L is therefore provided by drinking water. The advanced passive water harvesters, reported in literatures, normally demand 0.1-1 $m^2$ of solar panel area to effectively regenerate one kilogram adsorbent. Innovative designs in this field are constantly emerging, and the compactness of the AWH is anticipated to be improved in near future. Here, we assume that 0.2 $m^2$ solar panel area is sufficient to regenerate one kilogram adsorbent. On the other hand, the population density of the typical dense city Shanghai in China is 3923 per square kilometer. The per capita housing space of urban residents in Shanghai is 37.2 $m^2$. Therefore, assuming that no more than 20% of the floor area (about 3% of the land area) can be used to generate water, the minimum catchment ratio of the adsorbent will be sufficient:

$$0.2m^2/kg \times \frac{2.8kg}{\min\left\{\Delta W^i_{MOFs}\right\}} \leq 37.2m^2 \times 20\% \Rightarrow \min\left\{\Delta W^i_{MOFs}\right\} \geq 0.08g/g \quad \text{(Equation 35)}$$

Shanghai's average daily electricity consumption per person is 160kWh, of which 20% is residential electricity. Assuming that 5% of the residential electricity can be used to harvest water, the specific energy consumption to meet the minimum drinking water needs of an adult a day satisfies:

$$2.8kg \times \max\left\{SEC^i_{MOFs}\right\} \leq 160kWh \times 20\% \times 5\% \Rightarrow \max\left\{SEC^i_{MOFs}\right\} \leq 2MJ/kg \quad \text{(Equation 36)}$$

RSD measures the monthly distribution of water production. As shown in the Figure S24, the typical data density profile of one set of data with the RSD of 0.5 and the average value of 0.33g/g. This figure suggests the average value of the last 8% data is 0.08g/g, while the average value of the top 8% data is 0.58g/g. Namely, the maximum monthly water harvesting amount is almost 7 times of the minimum monthly water harvesting amount. As discussed before, AWH device is designed to generate at least 2.8 L water per capita in the worst month. As a consequence, with the RSD of 0.5, such device will generate 20 L water per capita in the best month. If

the RSD is larger than 0.5, the water distribution will become more separated, which means the device would generate 2.8 L water per capita under the worst condition but more than 20 L water per capita under best conditions. As discussed before, atmospheric water production more than 20 L per capita per day could be a waste. The RSD of 0.5 is therefore determined.

### Solar collector parameters

In this work, the desorption temperature is determined by the local solar radiation intensity. In order to increase the water extraction, we make the desorption temperature as high as possible by using solar collector panels. In the specification of this heat collector plate (Type: P-G/0.8-T/L/LT-1.82), we obtain the second order equation for its heat transfer.

$$\dot{Q} = A \cdot SR_{amb}\left(\eta - a_1\frac{\Delta t}{SR} - a_2\frac{(\Delta t)^2}{SR}\right) \quad \text{(Equation 37)}$$

Where Aperture area $A$ is 1.85m2; Conversion factor $\eta$ is 0.5; Heat transfer coefficient $a_1$ is 3.555; Temperature dependent heat transfer coefficient $a_2$ is 0.029. The solar energy collected by the solar collector becomes part of the solar energy that warms itself up, and the other part of the energy is transferred out, denoted as $\dot{Q}$. In our system, only a very small flow gap between the adsorbent and the solar collector is retained, so it can be assumed that the energy transferred out is 0. Equation 38 summarizes the equation for solving the relationship between the desorption temperature and solar radiation, and we give the image of the former term as a function of the solar radiation.

$$T_{d,DE} = \frac{\sqrt{a_1^2 + 4\eta \cdot SR_{amb}} - a_1}{2a_2} + T_{amb} \quad \text{(Equation 38)}$$

## QUANTIFICATION AND STATISTICAL ANALYSIS

We perform all our quantification and statistical analyses using MATLAB software (see key resources table). We report key statistical information to each analysis in the captions and legends of our figures and tables and describe specific calculation methods in the method details section.